

**Photoresponse of KNbO₃-AF₂O₃ (A = Bi³⁺ or La³⁺)
ceramics and its relationship with bandgap narrowing**

ELICKER, Carolina, PASCUAL-GONZALEZ, Cristina, GULARTE, Luciano,
MOREIRA, Mario, CAVA, Sergio and FETEIRA, Antonio
<<http://orcid.org/0000-0001-8151-7009>>

Available from Sheffield Hallam University Research Archive (SHURA) at:
<http://shura.shu.ac.uk/18966/>

This document is the author deposited version. You are advised to consult the publisher's version if you wish to cite from it.

Published version

ELICKER, Carolina, PASCUAL-GONZALEZ, Cristina, GULARTE, Luciano,
MOREIRA, Mario, CAVA, Sergio and FETEIRA, Antonio (2018). Photoresponse of
KNbO₃-AF₂O₃ (A = Bi³⁺ or La³⁺) ceramics and its relationship with bandgap
narrowing. *Materials Letters*, 221, 326-329.

Copyright and re-use policy

See <http://shura.shu.ac.uk/information.html>

1 **Photoresponse of KNbO₃-AFeO₃ (A = Bi³⁺ or La³⁺) ceramics and its relationship with bandgap**
2 **narrowing**

3

4 Carolina Elicker^{a,b,*}, Cristina Pascual-González^b, Luciano T. Gularte^a, Mario L. Moreira^a, Sergio S. Cava^a,
5 Antonio Feteira^b

6 ^a*Grupo de Pesquisa em Crescimento de Cristais Avançados e Fotônica, Universidade Federal de Pelotas,*
7 *Pelotas, Brazil.*

8 ^b*Christian Doppler Laboratory for Advanced Ferroic Oxides, Sheffield Hallam University, Sheffield,*
9 *United Kingdom.*

10 * Corresponding author. *E-mail:* carolinaelicker@yahoo.com.br

11

12 **Abstract**

13 The crystal structure of (1-x)KNbO₃-xBiFeO₃ (KNBF) and (1-x)KNbO₃-LaFeO₃ (KNLF) (where x=0.00;
14 0.01; 0.02; 0.04; 0.08; 0.16; 0.32) was evaluated by XRD and Raman spectroscopy. XRD data show the
15 crystal symmetry to evolve from orthorhombic to tetragonal with increasing *x*. The optical *bandgap* was
16 found to narrow systematically with increasing *x*. Raman spectroscopy analysis corroborated long-range
17 polar order in all compositions. The photoresponse of x=0.32 shows a typical diode-like behaviour, with
18 current and voltage of 0.115 μA and 0.075 V for KNBF and 0.19 μA and 0.035 V for KNLF, respectively.
19 To our knowledge these represent the largest values among KNbO₃-based ceramics, making them
20 promising for photovoltaic applications.

21

22 **Keywords:** *KNbO₃-based ceramics; bandgap narrowing; photoferroelectrics; ferroelectric photovoltaics.*

23

24 **1. Introduction**

25

26 The bulk photovoltaic effect in polycrystalline photoferroelectric materials it has long been
27 believed to be associated with the crystal polarity of these materials. Nevertheless, recently Yang et al[1]
28 suggested the bulk photovoltaic effect to actually originate from the non-centrosymmetry of ferroelectric
29 semiconductors and to be independent of the ferroelectric polarization. Typically most ferroelectrics exhibit

30 *bandgaps* of 3 eV or higher, thereby absorbing in the UV range.[2]. Tailoring their *bandgaps* in order to
31 achieve a maximum absorption around 1.5 eV, around the maximum of the solar spectrum, is therefore the
32 ultimate goal[3].

33 *Bandgap* engineering of ferroelectric potassium niobate (KN) is being studied by some
34 researchers. Pascual-González and co-workers[4] determined that the *bandgap* of $\text{KNbO}_3\text{-Bi(Yb,Me)O}_3$
35 (Me = Fe or Mn) narrowed by 1 eV for 95% $\text{KNbO}_3\text{-5%BiYbO}_3$. Later, the same authors found a narrowing
36 from 3.25 to 2.25 eV for 75% $\text{KNbO}_3\text{-25%BiFeO}_3$ compared to pure KNbO_3 [5]. Yu and co-workers[6]
37 studied the system $(1-x)\text{KNbO}_3\text{-xBa(Co}_{1/2}\text{Nb}_{1/2})\text{O}_3$ and noticed *bandgaps* as low as 2.4 eV for $x = 0.5$.
38 Grinberg and co-workers[7] studied the system $(1-x)\text{KNbO}_3\text{-xBa(Ni}_{1/2}\text{Nb}_{1/2})\text{O}_3$ and observed reduction by
39 more than 2 eV when increasing x . They also found short-circuit current and open circuit voltages of
40 ferroelectric photovoltaic device built with sample $x=0.1$ to be controlled by induced polarization.

41 This work presents the synthesis of $(1-x)\text{KNbO}_3\text{-xBiFeO}_3$ (KNBF) and $(1-x)\text{KNbO}_3\text{-xLaFeO}_3$
42 (KNLF) ceramics, their characterization and, for the first time, their application as a light harvesters in
43 ferroelectric photovoltaic (FEPV) devices.

44

45 **2. Materials and methods**

46

47 Pure KNbO_3 , $(1-x)\text{KNbO}_3\text{-xBiFeO}_3$ (KNBF) and $(1-x)\text{KNbO}_3\text{-xLaFeO}_3$ (KNLF) were
48 synthesized by solid-state reaction using K_2CO_3 , Nb_2O_3 , Fe_2O_3 , Bi_2O_3 and La_2O_3 (Sigma-Aldrich, purity
49 $\geq 99,00\%$, $99,90\%$, $99,99\%$, $99,99\%$ and $99,99\%$, respectively) as precursor materials. Powders were
50 weighed according the required molar ratios and mixed using a ball mill with Y-stabilized Zirconia balls
51 and isopropanol (Sigma-Aldrich). Slurries were dried, sieved and calcined twice in air at 800°C for 4h.
52 Finely milled powders were uniaxially-pressed into pellets under ~ 150 MPa and the green compacts were
53 sintered in air at 1075°C (KN), 1085°C (KNBF) and 1100°C (KNLF ceramics) for 4 h.

54 Purity and crystal structure analysis were carried out by X-ray diffraction (PANalytical™
55 Empyrean XRD, $\text{CoK}\alpha_1$ radiation). Crystal structure and long-range polarization were evaluated by Raman
56 spectroscopy (InVia, Renishaw, 532 nm solid state laser). *Bandgaps* were estimated from DRUV-Vis
57 spectra (Shimadzu, UV-3600 Plus) using the Wood and Tauc approach. Finally, ferroelectric photovoltaic
58 devices (FEPV) were fabricated with with a layout FTO/ferroelectric/electrolyte/Carbon/FTO, where FTO

59 is fluorine-doped tin oxide coated glass and the electrolyte is Redox-couple I/I_3^- . Carbon was painted
60 directly onto the FTO coated glass and the ferroelectric layer was deposited by casting. I–V measurements
61 were made under white light (210 – 1500 nm) (Ocean Optics, DH–2000) with a Keysight U2722A Source
62 Measure Unit.

63

64 3. Results and discussion

65

66 Fig. 1(a-d) shows the room-temperature XRD data for KNBF and KNLF ceramics. Pure KN
67 appears to be single-phase, with crystal symmetry described by the orthorhombic $Amm2$ space group.
68 Undoped KN exhibits the typical peak splitting expected for an orthorhombic perovskite, but within the
69 detection limits of the equipment, KNBF and KNLF display single peaks, as shown in Fig. 1(b,d).
70 Nevertheless, those peaks are clearly asymmetric, ruling out a simple cubic symmetry, as also corroborated
71 by the Raman spectra in Fig. 2. Indeed, KNBF up to $x=0.16$ and KNLF up to $x=0.08$ exhibit spectral features
72 consistent with orthorhombic symmetry. In KNBF $x=0.32$, orthorhombic and tetragonal crystal symmetries
73 coexist, in agreement with the recent work by Lennox and co-workers[8]. Similarly, for KNLF $x=0.16$, a
74 secondary tetragonal phase is also present, which appears to be in broad agreement with the work by
75 Kakimoto and co-workers[9].

76 Raman spectroscopy data shown in Fig. 2 corroborates the crystal symmetries suggested by the
77 XRD data. The typical spectral features exhibited by orthorhombic and/or tetragonal polymorphs are visible
78 in the spectra of all compositions, which can also confirm the occurrence of long-range polar order. In this
79 work, modes in the Raman spectra of KNBF and KNLF were assigned according to the classical work of
80 Shen and co-workers[10]. Within the resolution limits of the equipment, it is possible to observe, in the
81 low- to mid- wavenumber region of pure KN spectra: a (i) sharp mixed mode – $A_1(TO)$, $B_1(TO)$, $A_1(LO)$
82 and $B_1(LO)$ – at 193 cm^{-1} ; (ii) Fano-type interference dip at 199 cm^{-1} ; (iii) broad $B_1(TO)$ mode centered at
83 250 cm^{-1} ; (iv) $B_1(TO)$ at 275 cm^{-1} ; (v) sharp mixed mode – $A_1(TO)$ and $A_1(LO)$ – at 294 cm^{-1} . Modes (i),
84 (ii) and (v) are considered as "fingerprints" for long-range polar order. In the high wavenumber region it is
85 possible to observe a (vi) $B_1(TO)$ mode at 533 cm^{-1} ; (vii) $A_1(TO)$ mode at 600 cm^{-1} and; (viii) $A_1(LO)$ mode
86 at 834 cm^{-1} . KNBF ceramics present a broadening of the modes with increasing x , which can be associated
87 with the increasing of lattice disorder. A new shoulder neighbouring the sharp mixed mode at 193 cm^{-1} also

88 emerges. This new mode may be associated with A–O vibrations, in particular, with nanometric clusters
89 rich in K⁺ cations[5]. In KNLF $x=0.04$ ceramics it is possible to observe a sharp mode at $\sim 280\text{ cm}^{-1}$,
90 characteristic of the tetragonal polymorph[11]. For both KNBF and KNLF ceramics, the peak centered at
91 250 cm^{-1} shifts towards lower wavenumbers when increasing x , and a sharp mode emerges at $\sim 280\text{ cm}^{-1}$,
92 consistent with the orthorhombic-to-tetragonal phase transition[11].

93 The indirect optical *bandgaps* listed in Table 1 for KNBF and KNLF were determined using the
94 Tauc plots given in the Supplementary Information. Pure KN has a *bandgap* of $\sim 3.4\text{ eV}$. With increasing
95 x , the *bandgap* narrows continuously, for both KNBF, reaching 2.5 eV for $x=0.32$ (*i.e.* 26.5% reduction),
96 in agreement with the work by Pascual-Gonzalez and co-workers[5], whereas for KNLF $x=0.32$ the
97 *bandgap* narrows reaches 2.6 eV (*i.e.* 23.5% reduction). For KN, the excitation through the *bandgap* is a
98 charge transfer from the O 2p states at the top of valence band to the Nb 4d states at the bottom of the
99 conduction band[6]. For KNBF and KNLF compositions, the substitution Nb⁵⁺ by lower valence Fe³⁺ may
100 give rise to increased repulsion between the O 2p and Fe 3d states and thereby to a higher valence band
101 maximum, *i.e.* narrow *bandgap*. Additionally the disorder brought by Fe ions due to Fe 3d states, also
102 observed in high wavenumber region of the Raman spectra, which is sensitive to local depolarization
103 provide by Fe 3d and Nb 4d hybridization, may create localized states into the *bandgap*.

104 FEPV devices were fabricated from KNBF and KNLF $x=0.16$ and 0.32 . Current-tension (I–V)
105 curves obtained under dark and white light are shown in Fig. 3. Due to the non-linear electric behavior of
106 the FEPV devices, they were assumed as diodes[12] with shunt resistance (R_P) and series resistance (R_S).
107 While R_P can exist due to charge recombination and/or trapping, (R_S) of the system can be attributed to the
108 resistance of the interfaces ferroelectric/electrodes[13]. KNBF $x=0.16$ exhibits low diode-like behavior
109 (Fig 3a) with low open circuit voltage, 0.009 V and short circuit current of $0.12\text{ }\mu\text{A}$. KNLF $x=0.16$ (Fig.
110 3c) appear to have a linear dependence current/tension. Measured short circuit current and open circuit
111 voltage were $0.08\text{ }\mu\text{A}$ and 0.00022 V , respectively. Such linear behavior presented by both $x = 0.16$
112 indicates low R_P and high R_S , indicating that an enhancement in the interfaces ferroelectric/electrodes may
113 lead to an improvement of the FEPV device response. Particularly, for both $x = 0.32$ (Fig. 3b,d), the I–V
114 curves presented expected diode-like behavior, with low open circuit voltages and linear behavior in
115 photocurrent region (Fig. 3b,d, *inset*). Measured short circuit current and open circuit voltage were 0.115
116 μA and 0.075 V for KNBF and $0.19\text{ }\mu\text{A}$ and 0.035 V for KNLF. Changing to the shape of the I–V curves

117 with increasing x can be related to the presence of the tetragonal phase. Also the bandgap narrowing is a
118 reasonable explanation for photocurrent enhancement. This subject, however, needs further investigation.

119

120

121 **4. Conclusions**

122

123 It was demonstrated that the *bandgap* of KNBF and KNLF can be systematically narrowed by 0.9
124 eV (*i.e.* ~26.5% reduction) via replacement of K and Nb by Bi or La and Fe, respectively, without losing
125 long-range polar order. I–V measurements revealed 0.68KNbO₃–0.32BiFeO₃ and 0.68KNbO₃–
126 0.32LaFeO₃ to have diode-like behavior expected for solar cells. Moreover, KNBF and KNLF present
127 higher values of current compared to previous works in the literature[7]. Hence they are promising for
128 photovoltaic and optical sensor applications and require in-depth investigation.

129

130 **Acknowledgements**

131

132 The authors are thankful to CNPq, CAPES and FAPERGS, Grant Number 16/2551-0000525-7
133 for financial support. Carolina Elicker acknowledges CNPq for a SWE Scholarship (process no.
134 201665/2015–8). Cristina Pascual-González acknowledges Sheffield Hallam University for a VC doctoral
135 scholarship. Antonio Feteira is thankful to CNPq for a Special Visiting Researcher Fellowship. Giorgio
136 Schileo is acknowledged for the reflectance measurements. Cristian D. Fernandes is acknowledged for
137 sharing his expertise on I–V measurements.

138

139 **References**

140

141 [1] M.M. Yang, Z.D. Luo, D.J. Kim, and M. Alexe, Appl Phys Lett 110, (2017)183902.

142 [2] Y. Yuan, Z. Xiao, B. Yang, J. Huang, J Mater Chem A. 17 (2014) 6027-41.

143 [3] C. Paillard, X. Bai, I.C. Infante, M. Guennou, G. Geneste, M. Alexe, J. Kreisel, B. Dkhil, Adv Mater.
144 26 (2016) 5153-68.

145 [4] C. Pascual-Gonzalez, G. Schileo, A. Feteira, Appl Phys Lett. 13 (2016) 132902.

146 [5] C. Pascual-Gonzalez, G. Schileo, S. Murakami, A. Khesro, D. Wang I. M. Reaney, A. Feteira, Appl
147 Phys Lett. 17 (2017) 172902.

148 [6] L. Yu, J. Jia, G. Yi, Y. Shan, M Han, Mater Lett. 2016;184:166-168.

149 [7] I. Grinberg, D.V. West, M. Torres, G. Gou, D.M. Stein, L. Wu, G. Chen, E.M. Gallo, A.R. Akbashev,
150 P.K. Davies, J.E. Spanier, Nature. 503 (2013) 509-512.

151 [8] R.C. Lennox, D.D. Taylor, L.J.V. Stimpson, G.B. Stenning, M. Jura, M.C. Price, E.E. Rodriguez,
152 D.C. Arnold, Dalton Trans. 44 (2015) 10608-10613.

153 [9] K.I. Kakimoto, I. Masuda, H. Ohsato, J Eur Ceram Soc, 25 (2005) 2719-2722.

154 [10] Z. Shen, Z. Hu, T. Chong, C. Beh, S. Tang, M. Kuok, Phys Rev B. 52 (1995) 3976-3980.

155 [11] J. Baier-Saip, E. Ramos-Moor, A. Cabrera, Solid State Commun. 135 (2005) 367-372.

156 [12] Y. Liu, A. Hagfeldt, X.R. Xiao, S.E. Lindquist, Sol Energy Mater Sol, 1998;55:267-281.

157 [13] J.S. Agnaldo, J.B.V. Bastos, J.C. Cressoni, G.M. Viswanathan, Rev Bras Ens Fis. 28 (2006) 77-84.

158

159 **Figure Captions**

160

161 Figure 1 – X-ray diffractograms for KNBF and KNLF ceramics (a,c) and detailed peaks (b,d).

162 Figure 2 – Room-temperature Raman spectra for KNBF (a) and KNLF (b) ceramics.

163 Figure 3 – I–V curves for KNBF $x = 0.16$ (a), KNBF $x = 0.32$ (b), KNLF $x = 0.16$ (c) and KNLF $x = 0.32$

164 (d). Insets in each figure show detailed curves.

165

166

167

168

169

170

171

172

173

174

175 **Table Caption**

176

177 Table 1 - Indirect optical *bandgaps* for KNBF and KNLF ceramics.

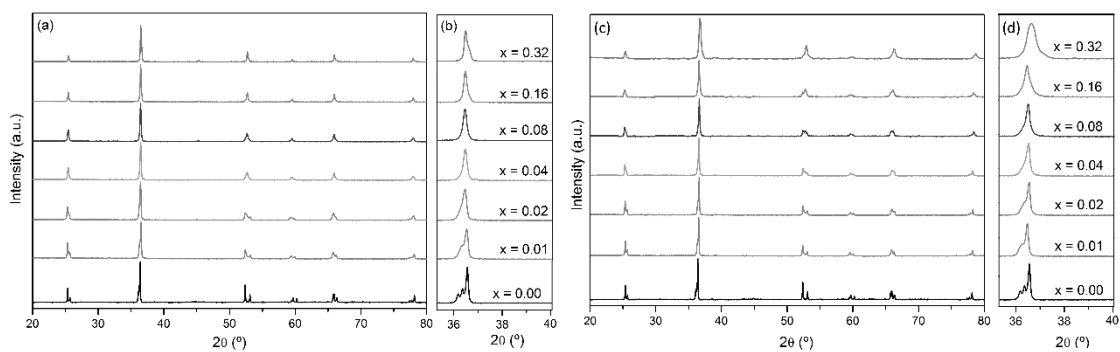
178

Composition	Bandgap (eV)
KN	3.40
KNBF $x = 0.01$	3.13
KNBF $x = 0.02$	3.12
KNBF $x = 0.04$	2.70
KNBF $x = 0.08$	2.60
KNBF $x = 0.16$	2.55
KNBF $x = 0.32$	2.50
KNLF $x = 0.01$	3.21
KNLF $x = 0.02$	3.20
KNLF $x = 0.04$	2.70
KNLF $x = 0.08$	2.68
KNLF $x = 0.16$	2.58
KNLF $x = 0.32$	2.60

179

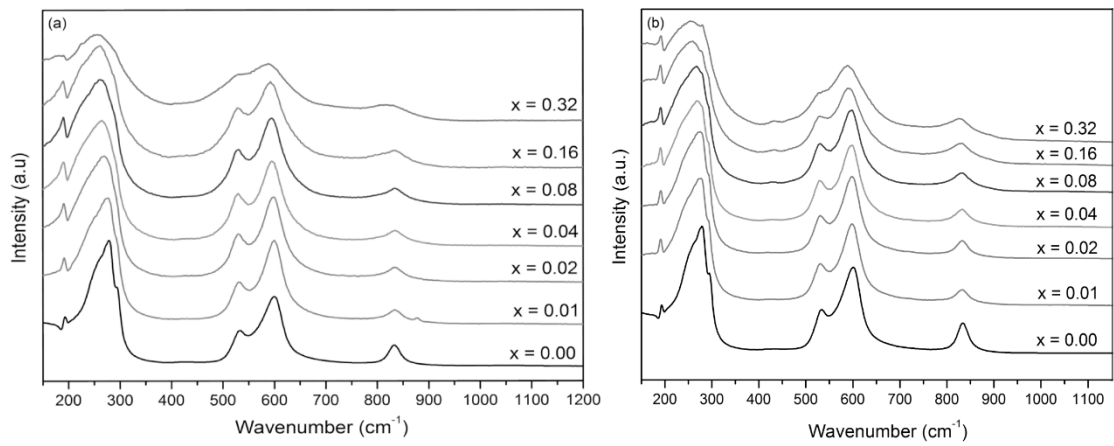
180

181



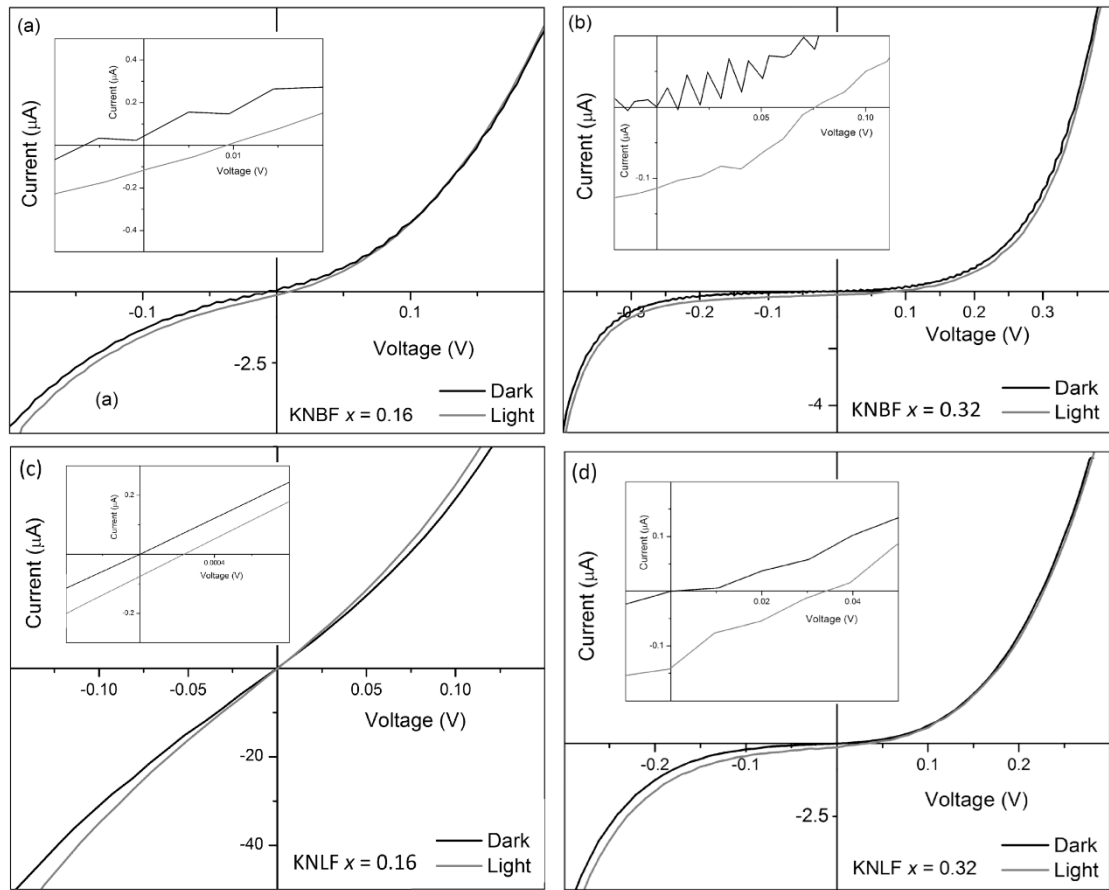
182

183 Fig. 1



184

185 Fig. 2



186

187 Fig. 3

188